Turing-Hopf front invasion: Rings and shells

Delora K. Gaskins, Jamie S. Soohoo, Irving R. Epstein,[*] and Milos Dolnik

Department of Chemistry, MS 015, Brandeis University, Waltham, Massachusetts 02453, USA

Invasion of Turing patterns into a region of bulk oscillations was investigated in the Belousov-Zhabotinsky-Aerosol OT reverse microemulsion system. Three distinct mechanisms for the formation of Turing structures at the expense of the bulk oscillation region were observed: frozen waves, which have been reported previously in this system, and reflecting waves and Turing-Hopf fronts, which have not. Turing-Hopf fronts appeared as the outer rings in this quasi-two-dimensional system with an amplitude intermediate between those of the Turing pattern and the phase waves in the bulk oscillation region. Three-dimensional (3D) Turing-Hopf shells (outer layers of 3D balls) were also observed.

Introduction. There are many examples of synchronized oscillations and pattern formation in the natural world as well as in engineered systems. Patterns form from a variety of fundamental instabilities and bifurcations, including the Hopf bifurcation and the Turing instability [1]. In the (supercritical) Hopf bifurcation, as the bifurcation parameter is changed the stable steady state becomes unstable and a stable limit cycle emerges, leading to oscillation of the system in time but not in space. In the classic case of the Turing instability, the uniform steady state is destabilized by the Fickian diffusion [2] of the components, and finite wavelength perturbations can grow, resulting in the development of patterns that are periodic in space, with an intrinsic wavelength, and stationary in time. The short-range-activation–long-range-inhibition paradigm that characterizes this instability can also be generated by other, nondiffusive spatial interactions [3].

It is possible to have bulk oscillations or Turing patterns that do not uniformly fill the domain (e.g., partial synchronization seen in chimera states [4] or localized Turing pattern domains [5]) and also to have coexistence of Hopf and Turing domains in a system with both bifurcations. Turing and Hopf bifurcations occur together in a variety of systems. They can be found in models of biological (predator-prey dynamics [6], neural activation [7]), physical (nonlinear optics [8], semiconductor [9]) systems, and, of course, chemical systems, which include the prototypical chlorite-iodide-malonic acid (CIMA) system for Turing pattern formation [2] and the Belousov-Zhabotinsky-Aerosol OT (BZ-AOT) system of our present study [10] as well as biochemical reaction networks [11] and electrodeposition [12]. When the Turing and Hopf instabilities interact, they can form patterns that are periodic both in time and in space. Some examples of mixed-mode Turing-Hopf (MM T-H) behavior are oscillatory Turing patterns [13,14] and oscillatory localized patterns [15], which been obtained in experiments on chemical reaction-diffusion systems.

Experiments on such systems supported by theoretical work have established that when one localized domain is embedded in or otherwise in contact with the other, the domain interface formed by the Turing pattern can be stationary [16–18] or it can move [15,18], leading to the growth of one pattern domain at the expense of the other. Theory predicts that these domain interfaces can reverse their direction of motion spontaneously at a critical parameter value [19,20] and that noise can increase the range within which destabilization can occur [21]. Recent experimental results have shown a phase-diffusion-like front between bulk oscillation and emerging Turing patterns [22]. MM T-H front structures between the domains have also been predicted [19].

Here we describe emerging Turing pattern domains that invade a region of bulk oscillation. Our major observation is the theoretically predicted MM T-H front structure, which we demonstrate by analyzing the amplitude (magnitude of brightness) of the pattern. In addition to the front structure, we observe different domain interface interactions, i.e., frozen wave dynamics [15] and a phenomenon that we dub reflecting waves.

Experimental. All reagents were purchased from Sigma-Aldrich, except AOT, which was obtained from ACROS Fisher. Two different microemulsion stock solutions were prepared in order to prevent the BZ chemical species from reacting prematurely. The first microemulsion (MEI) contained malonic acid (MA) and sulfuric acid, and the second (MEII) contained sodium bromate and ferroin. MEI and MEII contained equal amounts of 1.5 M AOT in cyclooctane. Both MEI and MEII were stirred for approximately 45 min. The microemulsions MEI and MEII were then combined at a 1:1 ratio, and cyclooctane was added to the resulting microemulsion to control the water droplet volume fraction (ϕ_d = [water]/[oil]). The time elapsed between combining MEI and MEII with cyclooctane and transferring the reacting microemulsion to the reactor was approximately 1 min. The concentrations of the BZ reactants for the aqueous phase of the reacting microemulsion were [malonic acid (MA)] = 0.25 M, [H_2SO_4] = 0.20 M, [$NaBrO_3$] = 0.20 M, and [ferroin] = 0.01 M. The [water]:[AOT] ratio of the reacting microemulsion (ω) was 12.347. While the patterns shown here have ϕ_d = 0.60, Turing-Hopf fronts were observed over a large range of lower ϕ_d values, down to 0.35.

―――――――
[*]epstein@brandeis.edu

The BZ-AOT system is able to produce a number of different types of qualitatively different patterns over its parameter space. Near the region where we report Turing-Hopf front formation, Turing patterns have been observed with $[MA] = 0.25$ M, $[H_2SO_4] = 0.20$ M, $[NaBrO_3] = 0.20$ M, $[ferroin] = 0.01$ M, $\omega = 13.9$, and $\phi_d = 0.348$ [10]. Dashed waves have been reported nearby in parameter space with $[MA] = 0.3$ M, $[H_2SO_4] = 0.2$ M, $[NaBrO_3] = 0.18$ M, $[bathoferroin] = 0.0049$ M, $\omega = 15$, and $\phi_d = 0.36$ [23] with segmented spirals at the same conditions with a different ϕ_d (0.71) [24]. It is thought that the interaction of excitable waves and the Turing instability is responsible for these segmented patterns [25]. Localized Turing rings have been observed previously in this system as well with $[MA]_w = 0.25$, $[H_2SO_4]_w = 0.25$, $[NaBrO_3]_w = 0.2$, $[bathoferroin]_w = 0.0049$. $[X]_w$ denotes the concentration of species X in the aqueous phase; $\phi_d = 0.41$ and $\omega = 15$ [15]. These patterns later developed into oscillons, and were suggested to be due to the subcritical Turing instability interacting with the Hopf instability.

We carried out quasi-two-dimensional (quasi-2D) experiments using two glass windows separated by a Teflon gasket of 0.09 mm thickness. The glass windows were contained in a sealed reactor body. Light was passed through the bottom of the reactor to allow images to be captured by a charge-coupled device (CCD) camera. Images were captured at one image per second. MATLAB was used to make space-time plots of the patterns and to determine the speeds of the Turing-Hopf fronts.

We employed a cylindrical quartz capillary with an internal diameter of 0.5 mm for the three-dimensional (3D) experiments [10]. This capillary was sealed and then submerged in an index-matching fluid (cycloctane). For reconstruction purposes, the capillaries were rotated at 4.5 s/revolution. Images (over several rotations at each time point) were acquired using CCD cameras. The inverse Radon transform was used in MATLAB in order to tomographically reconstruct the three-dimensional capillary and the pattern from the two-dimensional projections over one rotation [10].

Quasi-two-dimensional Turing-Hopf rings. Figure 1 shows the invasion of Turing patterns into a bulk oscillation domain
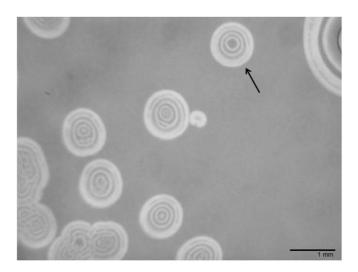

FIG. 1. Invasion of Turing patterns into the bulk oscillation region. The arrow indicates which Turing-Hopf ring is being followed in Fig. 2. The time elapsed is 526 s.
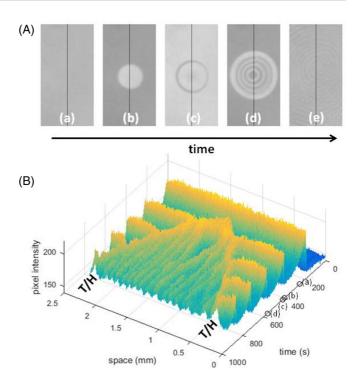

FIG. 2. Quasi-two-dimensional Turing-Hopf (T/H) front growth. (A) Bulk oscillations (a) are invaded by a localized spot (b) that survives an interaction with the next oscillation peak (c) to develop into Turing patterns behind the Turing-Hopf front (d). This pattern growth is one of the many shown in Fig. 1, the one the arrow points to. The final image shows the low-amplitude Turing patterns that remain after the front has invaded at (e) 1500 s. Images are 2.2×1.2 mm. The times corresponding to these images [(a) 250 s, (b) 397 s, (c) 417 s, (d) 562 s] are marked in part (B). (B) The amplitude of the line through the patterns in part (A) is plotted as a function of space and time (2.2 mm $\times$ 937 s).

via Turing-Hopf front rings in our quasi-two-dimensional reactor. The rings are the regions of bright amplitude (high concentration of oxidized catalyst) around the spots and spot pairs. There is also Turing-Hopf advancement from the bubble in the upper right corner. Figure 2 details the development of the indicated target-shaped invasion structure. Turing patterns are present within the rings while the bulk oscillation region is outside. An online video shows the time evolution of these patterns in the Supplemental Material [26].

Figure 2 shows in more detail the development of one of the spontaneously formed invasion centers in Fig. 1. Figure 2(A) shows the development of the pattern in space, with a uniform region giving way to a symmetry-breaking localized spot and then surviving a bulk oscillation. The fourth image in Fig. 2(A) shows the Turing rings that form behind the Turing-Hopf ring front. The last image of this sequence shows the low-amplitude Turing patterns that remain after many minutes in this batch system.

Figure 2(B) shows the behavior in time along a line through the localized spot in Fig. 2(A) and the surrounding region. Instead of the typical two-dimensional space-time plot with space and time axes, this is a three-dimensional rendering with the vertical axis representing the amplitude of the pattern, which is quantified using each pixel's grayscale intensity. A
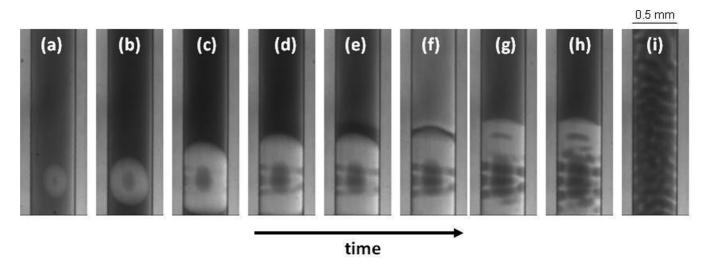
FIG. 3. A Turing-Hopf ball grows into a bulk oscillation domain. Images are 2D projections of the ball in the capillary at the following times: (a) 56 s, (b) 165 s, (c) 271 s, (d) 316 s, (e) 331 s, (f) 351 s, (g) 387 s, (h) 425 s, and (i) 1509 s. Turing patterns that remain after the growth of the front are shown at 1509 s.

parula color map in yellow, green, and blue is used to help with visualization of the amplitude intensity. The light regions in the images in Fig. 2(A) have higher pixel intensities and are more yellow in the false color of Fig. 2(B). Initially, the system is in a low-amplitude uniform state. Then there is the onset of bulk oscillations with a relaxational wave form seen along the right-hand edge of the space-time plot parallel to the time axis. The localized spot forms in the wake of the first bulk oscillation, failing to relax to the reduced minimum like the rest of the bulk. This spot maintains a relatively constant amplitude while growing in space. When the bulk reaches its second oxidation spike, it interacts with the localized spot, leaving a dark center in the spot surrounded by light rings. The innermost ring adjusts over time until the width of the dark center is the same as the wavelength of the rest of the ring Turing pattern. The outermost ring has an amplitude that is larger than that of the inner Turing pattern rings, but lower than that of the bulk oscillation. The amplitude of the front ring oscillates, which is most visible along the front edge furthest from the labeled time axis.

Three-dimensional Turing-Hopf balls and shells. Figure 3 shows Turing pattern invasion via Turing-Hopf front advancement in a three-dimensional reactor (capillary tube). These images encode the transmittance of light that passes through the capillary tube, rendering a projection of any three-dimensional structures within. A bright, not exactly spherical ball with a dark center is shown in Fig. 3(a), and this grows to touch the wall of the capillary [Fig. 3(b)]. Turing structures form on the wall as the front continues to advance along the vertical axis of the capillary tube as shown in Figs. 3(c) and 3(d). The bulk reaches the bright peak of its oscillation in Figs. 3(e) and 3(f), which retards the front growth briefly as the Turing patterns become more distinct just behind the front [Figs. 3(g) and 3(h)]. The front (shell) continues to advance and covers the reaction area, leaving Turing patterns in its wake. These patterns break up from stripes into spots over time, as seen in the final image in the figure.

Figure 4 also shows three-dimensional Turing pattern invasion via Turing-Hopf front advancement. As in Fig. 3, these

images show the transmittance of light that passes through the capillary tube, which allows one to see a projection of the three-dimensional structures within. Figure 3(a) shows half of a ball pinned to the wall of the capillary, a phenomenon seen more clearly in the isosurface from the reconstruction at this time in Fig. 5(a). The ball continues to grow and hollow out [Fig. 3(b)]. The bulk reaches its bright peak of oscillation, which interferes with the edge of the ball [Figs. 3(c) and 3(d)]. The front (shell) continues to advance [Figs. 3(e) and 3(f)] as the Turing patterns behind the front become more distinct. The reconstruction for the pattern in Fig. 3(f) is shown in Fig. 5(b). The last image in the sequence shows the Turing patterns that remain after the front advancement. The nearly parallel fronts near the bottom of the reactor result from a change from Turing-Hopf front advancement to Turing pattern domain growth via frozen waves.

Advancing Turing pattern domains. Turing pattern domains may invade bulk oscillation domains by several predicted and observed dynamical mechanisms. The most well-studied is the frozen wave mechanism, in which a phase wave slows to a stop as it approaches the established Turing pattern domain. When it stops, it becomes the outermost pattern stripe of the Turing domain. Frozen waves have been demonstrated in recent theoretical work by Berenstein and Carballido-Landeira [20], where they focused on developing an understanding of how abutting subdomains of Turing and bulk oscillations interact in a reactive microemulsion. Frozen waves have been reported in the BZ-AOT reactive microemulsion system with ferroin in octane and also in hexane [15].

A second mechanism of Turing advancement into bulk oscillation domains has the Turing pattern generating a phase wave. Turing spots in a quasi-one-dimensional system with the chlorite-iodide-malonic acid system have been observed to display this behavior [16]. Vanag and Epstein found a regime in the ruthenium-catalyzed BZ system where the outermost Turing pattern features generate phase waves behind which new fragments of Turing patterns emerge [15]. Turing-Hopf fronts generated in the FitzHugh-Nagumo model have also been predicted to generate phase waves as they advance [19].
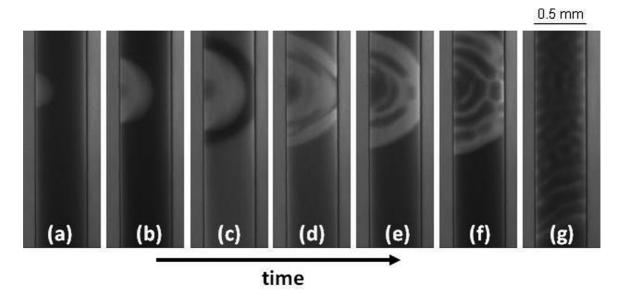
FIG. 4. Invasion by pinned Turing-Hopf half-ball. Images are the 2D projections of the half-ball in the capillary at the following times: (a) 118 s, (b) 238 s, (c) 285 s, (d) 329 s, (e) 369 s, (f) 502 s, and (g) 1569 s. Turing patterns that remain after the growth of the front are shown at 1569 s.

Our work (Fig. 2) clearly shows a Turing domain and a bulk oscillation domain separated by a front structure. It is evident from these two features that the system is in a region of parameter space where both a Turing instability and a Hopf bifurcation occur. However, the nature of the structure only becomes apparent on examining the amplitude of the front structure. The front structure oscillates but with an amplitude between those of the Turing amplitude behind the front and the oscillations in the bulk. This is evidence that the Turing and Hopf modes mix and that the front is a Turing-Hopf structure.

Or-Guil *et al.* [19] and Berenstein *et al.* [20] predict that the front can change directions for Turing-Hopf fronts and

with frozen waves. Frozen waves have been observed in a one-dimensional array of coupled oscillators where the front advancement is reversed via melting fronts [18]. We, in our batch system, observe a change from Turing-Hopf advancement to frozen wave advancement. The advancement of the front slows as the Turing patterns take over the Hopf domain (Fig. 2). During the transition between these two features, the advancing front meets the advancing phase wave and retreats, a behavior we dub a reflecting wave. The rings at the bottom of Fig. 4 show the planes added with each oscillation cycle for the frozen waves. The online video shows the three advancement mechanisms and the transitions between them in the Supplementary Material [26].

The slowing and transition of the front from advancing to retreating predicted by Or-Guil stems from the relative stability of the modes, and they established a dominance principle for this. The slowing of the front may be due to this relative stability of the Turing and Hopf modes. However, in our case, the transition to the frozen wave advancement mechanism is likely due to the aging of the solution in batch, which moves the system with respect to the codimension-two point.

Birth of the spatial structures. In this region of parameter space, shown by a typical example in Fig. 2, a uniform, nonoscillatory state is first observed, which then becomes unstable, leading to relaxation oscillations in the bulk.

The bulk oscillation becomes unstable to localized structures, which do not have a characteristic wavelength and show no discernible oscillations. The internal structure may collapse, creating a hole before or after the oxidation spike of the following bulk oscillation. The first Turing ring or internal ball forms around this region, and the patterns continue to grow in the form of rings left behind the advancing front. This can be more clearly seen in the video in the Supplementary Material [26].

Typically, Turing patterns arise from perturbations to the uniform steady state. However, the Turing patterns that form here do not do so from the uniform steady state. We interpret
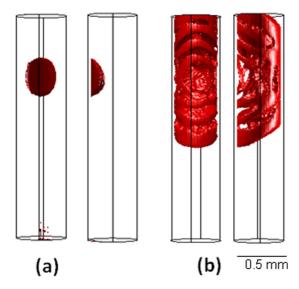

FIG. 5. Three-dimensional reconstruction of the Turing-Hopf half ball with panels (a) and (b) corresponding to the projections (a) and (f) in Fig. 4. The reconstructions are shown with their 90-deg rotations for clarity.

the destabilization of the bulk oscillations to give spatially localized structures to be a result of the Turing instability interacting with the Hopf bifurcation. Similar growth structures have been observed when localized Turing structures form and are embedded in a nonoscillatory domain in the subcritical Turing regime of the chlorite-iodide-malonic acid reaction [5]. Localized Turing rings that later develop into oscillons have been observed in this system not far away in parameter space [15]. Vanag *et al.* suggested that these might arise from the interaction of a subcritical Turing instability interacting with the Hopf instability.

Geometric considerations. In Fig. 1, a gas bubble can be seen in the upper right corner. In the supplemental video, we can see that along with the spot structures a light front begins to form at the interface of the bubble and the edge of the solution, an example of an edge effect [26]. This front behaves as the spots do, expanding away from the interface. The phase wave slows down as it approaches the edge, and patterns are generated behind that front. The two fronts meet and are replaced by a Turing stripe. Later, the outer front continues advancing away from the bubble. Edge effects are also possible in three dimensions, as shown by the pinning of the half-ball. We note that both the ball and the half-ball (Fig. 4) when they meet the boundary are traveling on a curved surface. Turing patterns on curved surfaces have attracted significant recent interest [27].

Or-Guil and Bode note that the honeycomb patterns generated by Turing-Hopf fronts in the FitzHugh-Nagumo model are much more regular and have fewer phase errors than the honeycomb planforms of the Turing patterns that appear from the steady state [19]. Perhaps the most striking feature about these Turing-Hopf fronts is the regularity of the Turing patterns that they lay down. In the two-dimensional case, concentric Turing stripes are left behind the front. Aligned Turing stripes generated from the Turing bifurcation are very

rare in BZ-AOT and CIMA. Typically in CIMA, Turing stripes are formed from labyrinthine patterns by using illumination as shown in Refs. [28] or [13]. Míguez and colleagues observed that there was a directional and velocity dependence of the stripes at the front, with stripes forming perpendicular to the front at the fastest front velocities. Frozen waves also align as stripes [15], as one stripe is added to the outer edge with each bulk oscillation.

Peña [28] used illumination to create stripes and also to force the resulting stripes so they underwent changes in morphology with the transverse zigzag instability, which was modeled with the Brusselator. In our supplemental video [26], the breakup instability can be observed as the stripes form spots, which remain. In addition, a transverse instability can be seen in the advancing fronts. These types of instabilities have been reported in the Gray-Scott model [29].

Conclusions. We have demonstrated by considering the amplitudes of the pattern components that Turing domains can advance into a bulk oscillation region following a Turing-Hopf front. We have shown this in two dimensions and explored what the three-dimensional analogs look like, for a ball that forms in the center of the cylindrical capillary and a ball that is pinned on the wall, both of which ultimately develop advancing Turing-Hopf front shells.

Pinning to the wall and other edge effects suggest a potential for planform control by strategic placement of barriers. Planform control could be useful for systems that have Turing and Hopf bifurcations, like electrodeposition at surfaces [12].

---

[1] A. M. Turing, Philos. Trans. R. Soc., B **237**, 37 (1952).

[2] V. Castets, E. Dulos, J. Boissonade, and P. De Kepper, Phys. Rev. Lett. **64**, 2953 (1990).

[3] D. Bullara and Y. De Decker, Nat. Commun. **6**, 6971 (2015).

[4] A. Schmidt, T. Kasimatis, J. Hizanidis, A. Provata, and P. Hövel, Phys. Rev. E **95**, 032224 (2017).

[5] P. W. Davies, P. Blanchedeau, E. Dulos, and P. De Kepper, J. Phys. Chem. A **102**, 8236 (1998).

[6] X. Tang, Y. Song, and T. Zhang, Nonlinear Dyn. **86**, 73 (2016).

[7] M. L. Steyn-Ross, D. A. Steyn-Ross, and J. W. Sleigh, Phys. Rev. X **3**, 021005 (2013).

[8] M. Ouali, S. Coulibaly, M. Taki, and M. Tlidi, Opt. Express **25**, 4714 (2017).

[9] W. Just, M. Bose, S. Bose, H. Engel, and E. Schöll, Phys. Rev. E **64**, 026219 (2001).

[10] T. Bánsági, V. K. Vanag, and I. R. Epstein, Science **331**, 1309 (2011).

[11] M. Mincheva and M. R. Roussel, Math. Biosci. **240**, 1 (2012).

[12] D. Laacitignola, B. Bozzini, and I. Sgura, Eur. J. Appl. Math. **26**, 143 (2015).

[13] D. G. Míguez, M. Dolnik, A. P. Muñuzuri, and L. Kramer, Phys. Rev. Lett. **96**, 048304 (2006).

[14] S. Alonso, D. G. Míguez, and F. Sagués, Europhys. Lett. **81**, 30006 (2008).

[15] V. K. Vanag and I. R. Epstein, Phys. Rev. Lett. **92**, 128301 (2004).

[16] J. J. Perraud, A. De Wit, E. Dulos, P. De Kepper, G. Dewel, and P. Borckmans, Phys. Rev. Lett. **71**, 1272 (1993).

[17] H. Willebrand, K. Matthiessen, F.-J. Niedernostheide, R. Dohmen, and H. Purwins, Contrib. Plasma Phys. **32**, 57 (1992).

[18] G. Heidemann, M. Bode, and H. Purwins, Phys. Lett. A **177**, 225 (1993).

[19] M. Or-Guil and M. Bode, Phys. A (Amsterdam, Neth.) **249**, 174 (1998).

[20] I. Berenstein and J. Carballido-Landeira, RSC Adv. **6**, 56867 (2016).

[21] S. Alonso and F. Sagués, Phys. Rev. E **80**, 035203 (2009).

[22] P. Dähmlow, V. K. Vanag, and S. C. Müller, Phys. Rev. E **89**, 010902 (2014).

[23] J. Carballido-Landeira, I. Berenstein, P. Taboada, V. Mosquera, V. K. Vanag, I. R. Epstein, V. Pérez-Villar, and A. P. Muñuzuri, Phys. Chem. Chem. Phys. **10**, 1094 (2008).

[24] V. K. Vanag and I. R. Epstein, Proc. Nat. Acad. Sci. USA **100**, 14635 (2003).

[25] A. Polezhaev and M. Borina, in *Nonlinear Dynamics of Electronic Systems*, edited by V. M. Mladenov and P. C. Ivanov (Springer, Cham, 2014), pp. 341–348.

[26] See Supplemental Material at http://link.aps.org/supplemental/10.1103/PhysRevE.98.040201 for video that shows the patterns developing in Fig. 1.

[27] G. Vandin, D. Marenduzzo, A. B. Goryachev, and E. Orlandini, Soft Matter **12**, 3888 (2016).

[28] B. Peña, C. Pérez-García, A. Sanz-Anchelergues, D. G. Míguez, and A. P. Muñuzuri, Phys. Rev. E **68**, 056206 (2003).

[29] T. Kolokolnikov, M. J. Ward, and J. Wei, Stud. Appl. Math. **116**, 35 (2006).